



Contents lists available at ScienceDirect

Journal of King Saud University – Science

journal homepage: [www.sciencedirect.com](http://www.sciencedirect.com)

Original article

## Green biosynthesized silver nanoparticles using *Acalypha wilkesiana* extract control root-knot nematode



Ahmed A. Heflish<sup>a</sup>, Amira E. Hanfy<sup>a</sup>, Mohammad Javed Ansari<sup>b,\*</sup>, Eldessoky S. Dessoky<sup>c</sup>, Attia O. Attia<sup>c</sup>, Moustafa M. Elshaer<sup>d</sup>, Mohamed K. Gaber<sup>e</sup>, Ahmed Kordy<sup>f</sup>, Ahmed S. Doma<sup>g</sup>, Ahmed Abdelkhalek<sup>h,\*</sup>, Said I. Behiry<sup>a</sup>

<sup>a</sup> Agricultural Botany Department, Faculty of Agriculture (Saba Basha), Alexandria University, Alexandria 21531, Egypt

<sup>b</sup> Department of Botany, Hindu College Moradabad (Mahatma Jyotiba Phule Rohilkhand University Bareilly) India-244001

<sup>c</sup> Department of Biology, College of Science, Taif University, P.O. Box 11099, Taif 21944, Saudi Arabia

<sup>d</sup> Department of Microbiology at Specialized Medical Hospital, Mansoura University, Egypt

<sup>e</sup> Plant Production Department, Faculty of Agriculture (Saba Basha), Alexandria University, Alexandria 21531, Egypt

<sup>f</sup> Plant Protection Department, Faculty of Agriculture (Saba Basha), Alexandria University, Alexandria 21531, Egypt

<sup>g</sup> Polymeric Materials Research Department, Advanced Technology and New Materials Research Institute, City of Scientific Research and Technological Applications, New Borg Al-Arab City, 21934 Alexandria, Egypt

<sup>h</sup> Plant Protection and Biomolecular Diagnosis Department, ALCRI, City of Scientific Research and Technological Applications, New Borg El Arab City, Alexandria 21934, Egypt

### ARTICLE INFO

#### Article history:

Received 2 April 2021

Revised 5 June 2021

Accepted 5 June 2021

Available online 11 June 2021

#### Keywords:

Ag NPs

Green biosynthesis

*Acalypha wilkesiana*

FTIR

SEM

Nematicidal activity

### ABSTRACT

Nanoparticles nowadays are an effective control agent against most phytopathogens. However, there are many reports on their antimicrobial activity and little as a nematicide. In this study, green biosynthesis of silver nanoparticles (Ag NPs) using *Acalypha wilkesiana* aqueous leaf extract was achieved. X-ray diffraction patterns confirmed the crystalline structure with face-centred cubic (fcc), where is the size was nearly 20 nm. SEM images of the Ag NPs show the spherical shape and in the range from 10 to 30 nm. Various functional groups, capping, and stability agents were identified using Fourier transmission infrared spectroscopy (FTIR). The nematicidal activity of biosynthesized Ag NPs conc. 25, 50, and 100 µg/mL were evaluated *in vitro* against root-knot nematode (*Meloidogyne incognita*), egg hatching (6 days after) and movement after 24 and 48 h. The Ag NPs (100 µg/ml) application after 48 h was the most effective treatment that showed 53.3% of nematode mortality. Overall, the efficiency of bio-Ag NPs reduced the nematode activity, mortality, egg hatching, and movement of larvae. To our knowledge, this is the first report of nematicidal action of biosynthesized Ag NPs using *A. wilkesiana* aqueous extract, and it could be recommended to manage the plant-parasitic nematode as it is simple, stable, cost-effective and keep the environment safe.

© 2021 The Author(s). Published by Elsevier B.V. on behalf of King Saud University. This is an open access article under the CC BY-NC-ND license (<http://creativecommons.org/licenses/by-nc-nd/4.0/>).

### 1. Introduction

Globally, plant diseases, in particular, are responsible for severe losses in crop production, which results in critical problems for food security (Abdelkhalek et al., 2020a; Abo-Zaid et al., 2020). Plant-

parasitic nematodes are among the most critical and dangerous pests attacking various plants in conventional and organic farming systems (Abd-El-Kareem et al., 2021; Khan et al., 2021). It has been estimated that the plant-parasitic nematodes annually contribute to significant economic losses of around 173 billion dollars in damage to crop production yield and quality worldwide. Different species of root-knot nematodes (*Meloidogyne* spp.) include *M. arenaria*, *M. javanica*, *M. hapla*, and *M. incognita*, are considered to be the most common species responsible for 90% of the predictable damages, with a significant impact on field and vegetable crops (Khan and Kim, 2007). All plant parts, such as bulbs, roots, rhizomes, buds, flowers, and seeds, are infected by nematodes.

*M. incognita* belongs to the family *Meloidogynidae*, and it is widely known as root-knot nematode because it favours root

\* Corresponding authors.

E-mail addresses: [mjavedansari@gmail.com](mailto:mjavedansari@gmail.com) (M.J. Ansari), [aabdelkhalek@srtacity.sci.eg](mailto:aabdelkhalek@srtacity.sci.eg) (A. Abdelkhalek).

Peer review under responsibility of King Saud University.



Production and hosting by Elsevier

<https://doi.org/10.1016/j.jksus.2021.101516>

1018-3647/© 2021 The Author(s). Published by Elsevier B.V. on behalf of King Saud University.

This is an open access article under the CC BY-NC-ND license (<http://creativecommons.org/licenses/by-nc-nd/4.0/>).

attacking. Several methods such as soil fumigation, nematicides, and cultivars resistant to the nematode were reported to control the *M. incognita*. Commercial nematicides are the primary management strategy to reduce the nematode effect in the infested crops; however, these commercial products have been harmful to humans (Abdelkhalek et al., 2020c; Cromwell et al., 2014). Moreover, due to the problems associated with environmental pollution, residual toxicity, and public health hazards, the use of chemical nematicides is objectionable (Cromwell et al., 2014).

Nanotechnology has an excellent inspiration for biological sciences and life science (Hassan et al., 2021). Nanomaterials, in a nanoscale range (1 nm to 100 nm), have high momentum in recent years due to their wide applications, including medicine, environmental science, food processing, and agriculture (Abdelkhalek and Al-Askar, 2020; Ghramh et al., 2019; Khan et al., 2019). In agriculture, nanoparticles utilization increased plant resistance to plant microbes, promote plant growth, reduced disease severity, increased crop production, and inhibit pathogen infection (Masry et al., 2021). Moreover, induction of systemic acquired resistance (SAR), which associates with the increase in antioxidant activity, was observed (Abdelkhalek and Al-Askar, 2020).

Due to their unique physicochemical properties, antioxidant and antimicrobial, silver nanoparticles (Ag NPs) are considered one of the most attractive nanomaterials utilized in different life sciences applications (Aziz et al., 2019). Ag NPs have potential recognized in tremendous applications in medical diagnostics, pharmacology, and agriculture and extensively reviewed in the literature (Joshi et al., 2018). Ag NPs have demonstrated efficacy against many plant pathogens, including bacteria, fungi, viruses, and nematode (Nassar, 2016).

Several chemical and physical methods were used to obtain nanoparticles, such as chemical reduction of silver salt solution, ultrasonication, microwave irradiation, solid-state thermal decomposition, and laser vaporization (Kharissova et al., 2013). Such techniques require expensive equipment, high energy, and space. Besides, the requirement of the capping agents for size stabilization constituted a costly and toxic method making it toxic for the environment and unsuitable for many biological and agriculture applications (Ouda, 2014). Nowadays, the green or biological biosynthesis methods of nanoparticles have been suggested as safe alternatives to the physical and chemical methods. They offer simplicity in the process of synthesis, cost-effective, eco-friendly, biocompatible with nature (Alamdari et al., 2020). Such biological methods of Ag NPs synthesis used microorganisms (including fungi, bacteria) and plants products or extracts as reducing agents in the biosynthesis processes (Bhuyan et al., 2015).

In the present study, we target to green biosynthesis of Ag NPs using *A. wilkesiana* aqueous extract as a stabilizing agent. Moreover, x-ray diffraction (XRD), scanning electron microscopy (SEM), fourier transform-infrared spectroscopy (FTIR), particle size analyzer (PSA), as well as zeta potential (ZP) were used to study the biosynthesized Ag NPs. Additionally, the nematicidal action and the efficiency of bio-Ag NPs to reduce the activity of nematode; mortality, egg hatching, and movement of larvae were tested. To our knowledge, this the first study of the nematicidal action of biosynthesized Ag NPs from *A. wilkesiana* aqueous extract against plant root-rot nematode.

## 2. Materials and methods

### 2.1. *Acalypha wilkesiana* leaves aqueous extract preparation

Fresh leaves of *Acalypha wilkesiana* were collected from the Faculty of Agriculture, Saba basha, Alexandria University, Egypt

(Fig. 1). To remove debris and other contaminations, the collected leaves were washed thoroughly with tap water, washed three times with ultrapure Milli Q water and air-dried for one week at room temperature. A sterile electric blender milled the dried leaves into powder. *A. wilkesiana* aqueous extract was prepared by mix 10 g of leaf powder with 100 mL of de-ionized sterile water, followed by stirring for 2 h at 60 °C. After cooled at 25 °C, the solution was filtered through sterile Whatman No. 1 filter paper and kept on the fridge for further use.

### 2.2. Green synthesis of silver nanoparticles

A 1 mM aqueous solution of silver nitrate was prepared via dissolving 0.0169 g of AgNO<sub>3</sub> (Sigma Aldrich, USA) in 100 mL double distilled water. A 10 mL of aqueous *A. wilkesiana* leaves extract was added to 90 mL of AgNO<sub>3</sub> solution freshly prepared for reduction AgNO<sub>3</sub> into Ag<sup>+</sup> ions. The solution was well mixed and put on a shaker until the observation of color change. The appearance of a reddish-brown color indicated the formation of Ag NPs. Optical density was recorded at regular intervals of time using a UV-V spectrophotometer until the reading peaked (color became dark yellow). The solution after that was centrifuged for 20 min at 5.000 rpm, then the pellet (Ag NPs) washed with sterile distilled water three times followed by wash with ethanol to get rid of the impurities. Then, the obtained Ag NPs dried at 50 °C in an oven and subjected for further physical and biological characterization.

### 2.3. XRD analysis

XRD patterns were registered in (Shimadzu XRD-6100) diffractometer, using CuK $\alpha$  radiation ( $\lambda = 1.5406\text{\AA}$ ), (40 kV and 30 mA conditions). Data were collected over the  $2\theta$  range of 5–90°, 0.0200 steps, and 10 s counting time per step. The average crystallite size (D) of Ag NPs calculated using the Debye–Scherer formula:

$$D = \frac{K\lambda}{\beta \cos\theta} \quad (1)$$

the value of  $d$  the interplanar spacing between the atoms and the expected  $2\theta$  positions are calculated using Bragg's Law:

$$n\lambda = 2d\sin\theta, \quad (2)$$

where  $\theta$  is the incident angle,  $d$  is the distance among atomic layers in a crystal, the variable  $\lambda$  is the wavelength of the incident X-ray beam, and  $n$  is an integer (El-Khatib et al., 2018). The distance  $d$  was defined by

$$1/d^2 = \frac{K^2 + h^2 + l^2}{a^2}$$



Fig. 1. *Acalypha wilkesiana* plant.

where  $a$  is unit cell parameter,  $(h\ k\ l)$  are miller indices.

#### 2.4. Scanning electron microscopy, Fourier transforms infrared spectroscopy and particle size analyzer

The morphological, surface and shape, structures and size of Ag NPs were characterized by scanning electron microscopy (SEM) at 10 kV (JSM-6360 LA, JEOL, Tokyo, Japan), and the working distance was adjusted to around 3 mm. Fourier transforms infrared spectroscopy (FTIR) were obtained with FTIR-8400S SHIMADZU, with the KBr disc method to investigate different functional groups of the prepared extract. The particle size analyzer instrument (MALVERN, ZETASIZER Ver.6.20) used to analyze the particle size distribution. The sample was analyzed in quartz. Thet, the temperature was adapted at 25 °C, and pure water was used for the viscosity and refractive index values, which allows an excellent size resolution. PCS is a method focused on the interaction between light and particulates. The light scattered by nanoparticles in suspension was fluctuated with time and associated with particle diameter. Diffracted intensity is proportional to of atoms number in a cluster.

#### 2.5. Zeta potential measurements of Ag NPs

The size distribution of the particle of bio-Ag NPs was determined using dynamic light scattering (DLS) with Malvern–Model Zeta sizer Nano ZSP which is used to control the stability of the sample. Nanoparticles samples in liquid structure (5 mL) were diluted twice with the distilled water quantity (50 mL), and then adjusted the pH to the desired value. After shaking samples for 30 min, the zeta potential of the metallic particulates was measured. The Zeta potential (ZP) was measured by determining the electrophoretic mobility

$$E = \frac{V}{d} \quad (4)$$

and then by applying the Henry equation (Griffiths et al., 2011), ZP can be calculated:

$$\text{Zeta Potential (ZP)} = \frac{\mu\eta}{\epsilon_0\epsilon_r} \quad (5)$$

where  $\mu$  is electrophoretic mobility of silver,  $\epsilon_0$  the permittivity of free space,  $\epsilon_r$  is sample permittivity and  $\eta$  is the viscosity of the solution

#### 2.6. Collecting, identifying, and enumerating nematode

*M. incognita* root-knot nematode populations were isolated from infected roots of weed *Solanum nigrum* L. (Wolf's grapes or Black Nightshade) which belongs to the family *Solanaceae* with heavy galls, collected from the governorate of El-Beheira, Egypt. Using original descriptions and diagnostic keys, processed females and species' temporary and permanent mounts were described under a stereomicroscope (JN, 1985). The Extraction of eggs from infected roots of *S. nigrum* was obtained by washing the infected roots with tap water to remove the soil and debris, and then the washed roots chopped into small pieces (1 cm). About 100 g of the infected roots were shaken vigorously for 2 min in a jar containing sodium hypochlorite (NaOCl) solution (0.5%) and then poured through a 250- $\mu$ M mesh sieve to collect the eggs. The collected eggs used to further purification to eliminate eggs containing fractions by rinses with sterile distilled water to have purified egg suspension (Hussey, 1973). The average density of nematode eggs in the suspension thus prepared counted using the light microscope; the average was represented for the number of eggs in suspension.

#### 2.7. Effect of Ag NPs on nematode under laboratory conditions

The effect of Ag NPs was evaluated on *Meloidogyne* spp. under laboratory conditions. Bio-Ag NPs of (25, 50, and 100  $\mu$ g/ml) concentrations were prepared with distilled water. Effects of Ag NPs on egg hatching; 1 mL of root-knot nematode eggs suspension added to 1 mL of Ag NPs. Distilled water without egg suspension was used as a control. All treatments have been sustained at  $28 \pm 2$  °C. The numbers of hatched eggs in the treatments were counted after 6 days. As a mean percentage of dead nematodes, the effect of bio-Ag NPs was expressed. Five replicates were used for each treatment. After six days, the number of hatched juveniles was counted.

Effects of Ag NPs (25, 50, and 100  $\mu$ g/ml) on *Meloidogyne* mortality and movement were evaluated under laboratory conditions. Suspensions of *Meloidogyne* juveniles were prepared in distilled water. One ml of nematode suspension was added to 1 mL of Ag NPs, and 3 mL distilled water mixed in sterilized Petri dishes. Distilled water instead of Ag NPs was used as a control, and five replicates were used for each treatment. Petri dishes of the treatments were incubated at  $28 \pm 2$  °C. After 1 and 2 days, the numbers of dead juveniles were counted, and the toxicity of Ag NPs was calculated as the percentage of dead nematodes. The movement was used as an indicator of nematodes mortality (Abbasi et al., 2008).

### 3. Results and discussion

#### 3.1. X-ray diffraction (XRD) analysis

Generally, XRD applied to investigate the phase and crystallographic structure of the biosynthesized Ag NP. Fig. 2 showed the XRD pattern of Bio-Ag NPs. The actual pattern was modified to show four sharp diffraction peaks. The main peaks at  $(2\theta)$  38.61, 44.85, 65.28, and 78.12 correspond to the (111), (200), (220), and (311) planes, respectively. By comparing JCPDS (file no: 89-3722), the typical pattern of biosynthesized Ag NPs is found to possess an fcc structure. The sharpening of the peak indicates that the particles are in the nano region. The intense high peak for face-centred cubic material (fcc) is (111), which is observed in the powdered sample and indicated that spherical bio-Ag NPs had the top plane with (111). Peaks were indexed using JCPDS files (JCPDS card no.: 89-2838) (El-Khatib et al., 2020). XRD characteristics are listed in Table 1. From XRD values, this prominent peak, d-Spacing, and expected  $2\theta$  for bio-Ag NPs are listed in Table 2. Overall, the results confirm that the biosynthesized Ag NPs were crystalline in nature.

#### 3.2. Fourier transforms infrared spectroscopy (FTIR) analysis

Generally, plant extracts are an eco-friendly effective biocontrol agent against a wide range of plant pathogens (Abdelkhalek et al.,

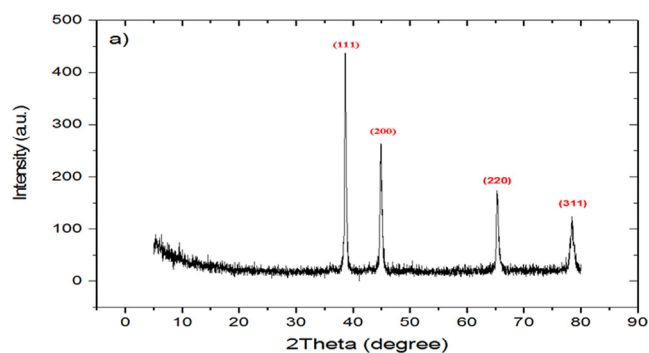


Fig. 2. X-ray diffraction (XRD) spectrum of biosynthesized silver nanoparticles.

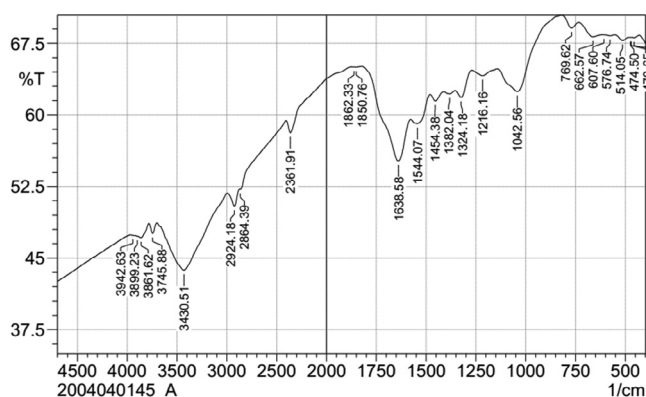
**Table 1**  
X-ray parameters for Ag NPs.

Diffraction angle (2 $\theta$ )	I/I <sub>0</sub>	d (Å)	(h k l)	Full width at half maximum (FWHM)	D (nm)
38.65°	105	2.31	(111)	0.24	0.42
44.81°	59	2.04	(200)	0.34	21.2
65.22°	31	1.4	(220)	0.33	28.81
78.19°	18	1.26	(311)	0.29	27.41

**Table 2**  
Distinguished calculated peaks, d-spacing and the expected 2 $\theta$  positions of Ag NPs.

2 $\theta$ Measured (°)	d-spacing corresponding value	The expected 2 $\theta$ positions (°)
38.65	0.2337	35.14
44.81	0.1991	41.72
65.22	0.1411	57.70
78.19	0.1231	71.82

2020b). Due to its secondary metabolites such as carbohydrates, polyphenols, esters, polysaccharides, and terpenoids, many plant extracts were reported as reducing agents in the nanoparticles synthesis processes (Joshi et al., 2018). FTIR spectroscopy was used to recognize the functional groups in the Ag NPs solutions. Thus, it helps to identify the possible biomolecules responsible for the reduction of Ag<sup>+</sup> ions (Ansari et al., 2013). In the current research, it was found that the secondary metabolites of *A. wilkesiana* were responsible for reducing Ag<sup>+</sup> into Ag NPs. The FTIR spectrum of the biosynthesized Ag NPs presented several peaks (Fig. 3). The broad peak at 3430.51 cm<sup>-1</sup> indicated the presence of hydrogen-bonded groups and could be corresponded to hydroxyl groups (O–H) and/or N–H (amine) stretching out from the phenolic compounds that were existed in the plant extract (Alamdari et al., 2020). Likewise, the peaks at 3942.63–3745.88 cm<sup>-1</sup> representing stretching vibration of O–H group Mohammadi-Aloucheh et al., 2018). The bands were seen at 2924.18, and 2864.39 cm<sup>-1</sup> are due to C–H stretching. The band at 2361.91 corresponded to O=C=O (carbonyl bond group). The peak seen at 1638.58 cm<sup>-1</sup> assigned to N–H (amine) bends (Gupta et al., 2018). The peaks at 1544.7 and 1042.65 represent C–H (alkane) bend and C=O (alcohol/ether) stretching, respectively. The results agree with Dada et al. (Dada et al., 2019) who reported that the presence of flavonoids, saponins, triterpenes and phenols responsible for bioreduction of Ag<sup>+</sup> to and stability of Ag NPs. Moreover, the phytochemical analysis of the aqueous leaf extract of *A. wilkesiana* showed that presence of flavonoid, carbohydrates, tannins in high percent.

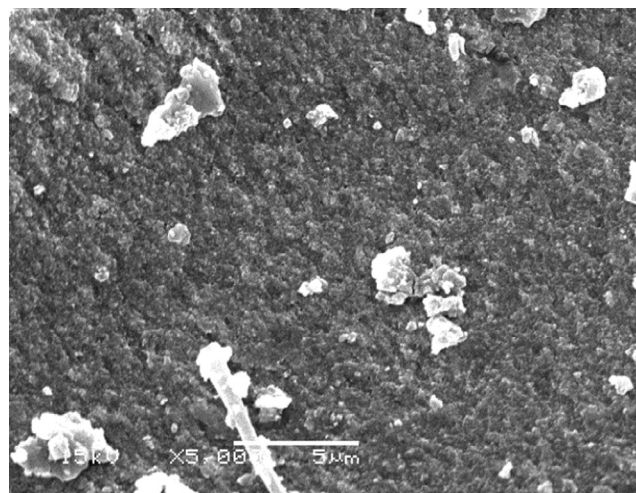
**Fig. 3.** FTIR spectra of Ag NPs biosynthesized by *A. wilkesiana* leaf extract as reducing agents.

### 3.3. Particle size distribution and scanning electron microscopy analysis

Dynamic light scattering (DLS) is a technique commonly used to determine the size distribution profile of particles in a colloidal solution (Kulikov and Koshlan, 2015). In the present study, DLS analysis revealed that the particle size distribution of the biosynthesized Ag NPs in the aqueous medium was broad, but a single peak distribution related to the average particle size looked at 25.7 nm (Fig. 4). Scanning electron microscopy (SEM) is one of the most powerful methods for surface morphological examination with direct visualization of the nanoparticles. SEM results indicated that the less miscible prepared powders are made of pure Ag NPs, which appear as spherical particles (Fig. 5). It is evident from the SEM images that Ag NPs were agglomerated. This could be attributed to the free static charges at the Ag NPs surface. These SEM images indicated the evidence of nanostructure with a few large round particles; before the biosynthesis method. It produces single-crystalline Ag NPs. The particle diameter range was between 10 and 30 nm. SEM analysis confirmed the morphology and size of the previously prepared Ag NPs (Datta et al., 2017). SEM results showed that the primary particles have a rather broad size distribution, which is in good agreement with particle size distribution result.

### 3.4. Zeta potential analysis

Zeta potential is an analytical technique applied to determine the surface charge of nanoparticles in solution. In the current study, the Zeta value of the Ag NPs was measured and found to be -16.1 mV at pH = 7 (Fig. 6). This value indicating a negative charge over the prepared Ag NPs surface when dispersed in water and provides satisfactory evidence about their little tendency towards aggregation when its negative charges with a diameter of 16.1 nm (Fig. 6). This behaviour suggests the existence of strong electric charges on the surfaces of Ag NPs to hinder agglomeration.

**Fig. 4.** Particle size distribution of biosynthesized Ag NPs.

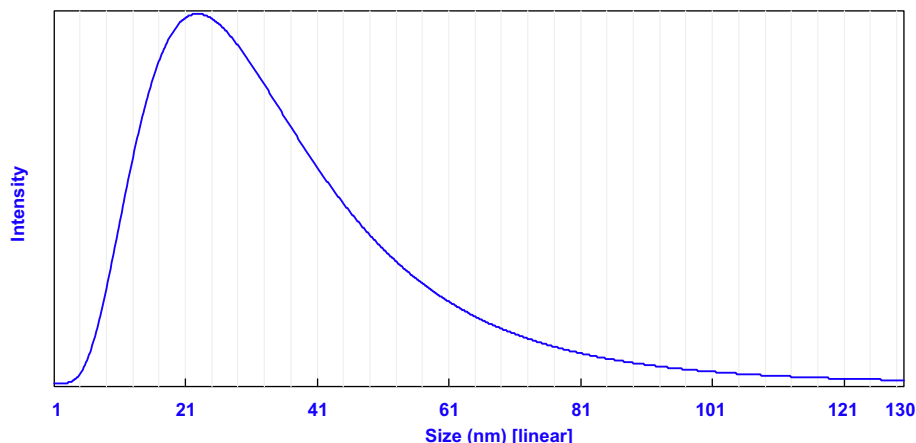


Fig. 5. SEM images of silver nanoparticles biosynthesized by *A. wilkesiana* leaf extract as reducing agents. (Bar = 1  $\mu\text{m}$  at  $\times 5,000$ ).

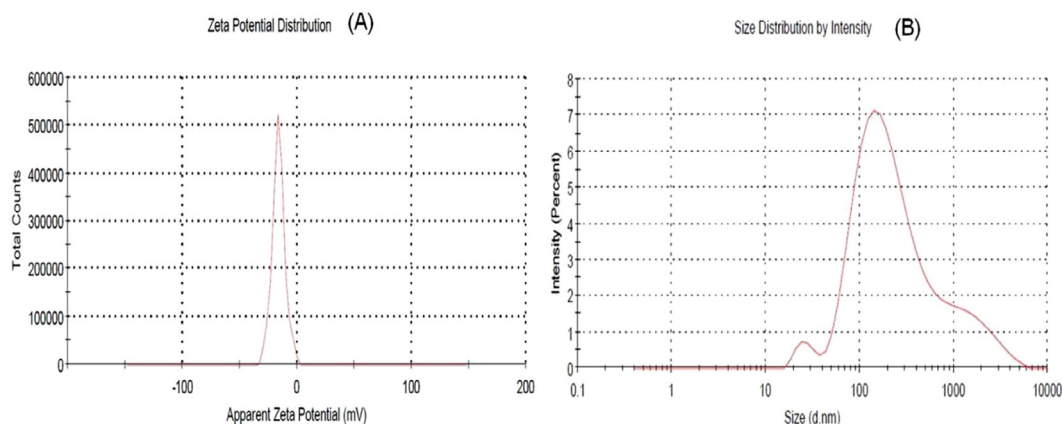


Fig. 6. (a) Zeta potential analysis of Ag NPs and (b) Dynamic light scattering analysis of Ag NPs.

The negative value proved the capping materials efficiency in stabilizing Ag NPs by introducing enough negative charges that keep all the particulates away from each other (Haider and Mehdi, 2014). The negative charge present on the surface causes repulsion between Ag NPs particles leading to more stability with uniform distributions state in solution. These negative charges might be due to bioactive molecules in the *A. wilkesiana* leaf extract that was proven by FTIR analysis. Similar results were reported in leaf derived Ag NPs of *Peltophorum pterocarpum*, *Saraca indica*, *Petalium murex* and *Hyptis suaveolens* ((Mukherjee et al., 2016; Botcha and Pratiapati, 2019).

### 3.5. Efficacy of Ag NPs on egg hatching and mortality percentage of nematode

The effect of biosynthesis Ag NPs (25, 50 and 100  $\mu\text{g}/\text{mL}$ ) on egg hatching after 6 days and mortality percentage of root-knot nematode (*M. incognita*) after 24 and 48 h presented in Fig. 7. The results showed a significant effect of the nanomaterial reduction of nematode eggs hatching. Data showed that 100  $\mu\text{g}/\text{mL}$  concentrations revealed the highest reduction of juveniles from eggs and the lowest number of egg hatched 7.6%, while 50  $\mu\text{g}/\text{mL}$  and 25  $\mu\text{g}/\text{mL}$  increase the egg hatching; 12.66 and 17.72%, respectively. The mortality percentage of root-knot nematode after 24 h, 100  $\mu\text{g}/\text{mL}$  perceived gave the highest mortality percentage (48.9%) while the lowest Ag NPs concentration, 25  $\mu\text{g}/\text{mL}$ , was 3.9% compared

with control (distilled water). Data showed that the mortality percentage was increased with increasing the Ag NPs concentration (Fig. 7). On the other hand, after 48 h. of treatment, 100  $\mu\text{g}/\text{mL}$  concentrations also displayed the highest mortality %, 53.3%. In contrast, 50  $\mu\text{g}/\text{mL}$  of Ag NPs offered 50.9 mortality %, more than 25  $\mu\text{g}/\text{mL}$ , which offered 3.7 mortality %. The results showed an increase in nematode mortality from the lowest concentration (25  $\mu\text{g}/\text{mL}$ ) to the highest one (100  $\mu\text{g}/\text{mL}$ ). The nematicidal effect of Ag NPs against root-knot nematodes was considered and studied in previous works). The treatment with bio-Ag NPs revealed the highest mortality percentage, and it could be a powerful tool in combating the root-knot nematodes. The data displayed revealed abnormal embryogenesis, abnormal larvae and paralyzed larvae under the light microscope 10X (Fig. 8). These findings were in line with the previous work of Cromwell et al. (Cromwell et al., 2014), who reported that using Ag NPs (30–150  $\mu\text{g}/\text{mL}$ ) against *M. incognita* showed 99% mortality after six hours. On the other hand, using high levels from Ag NPs (500 ppm and 1000 ppm) found to be significantly effective on nematode reproductively (Taha and Abo-Shady, 2016). It is clear from obtained results that Ag NPs inhibited *M. incognita* development and hatching. From the previous studies, it's not clear the mode of action of Ag NPs, but it can be linked with ATP synthesis in the cell, the permeability of the membrane, and its response to oxidative stress in prokaryotic and eukaryotic cells, as found by previous researchers (Ahamed et al., 2010). These findings could make the biosynthesized Ag NPs an effective eco-

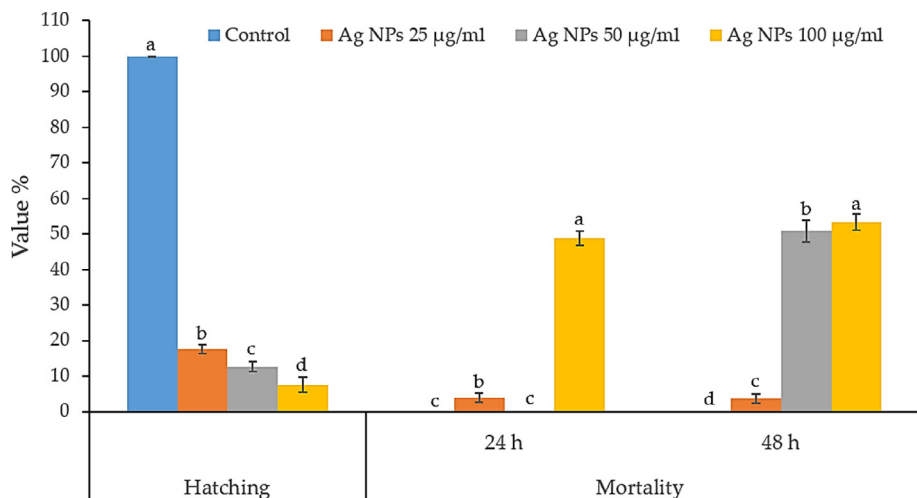


Fig. 7. Effect of Ag NPs on the percentage of hatching nematode after 6 days and nematode mortality after 24 and 48 h of treatments.

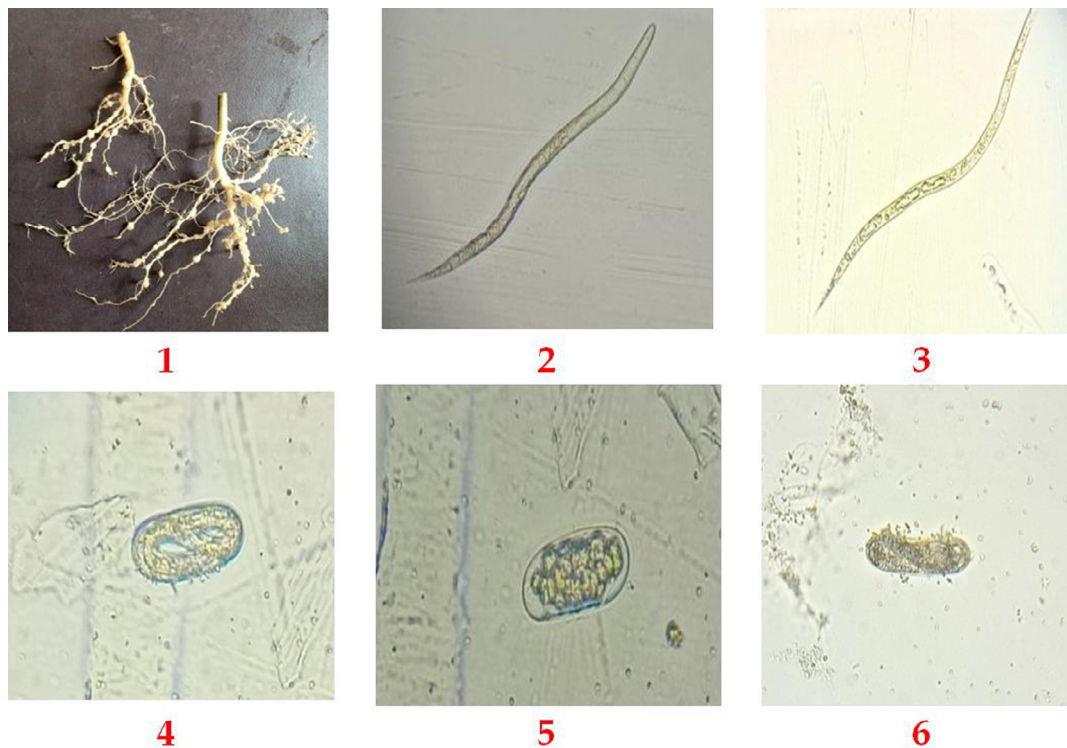


Fig. 8. Displaying the effect of Ag NPs on root-knot nematode; (1) infected roots of *Solanum nigrum* L plant, (2) typical nematode larva, (3) paralyzed larvae (4) regular nematode eggs, (5) abnormal or paralyzed juvenile in eggs and (6) destroyed nematode eggs.

friendly method to control root-knot nematode in small doses compared with the highest doses of chemical nematicides.

### 3.6. Effect of Ag NPs on the movement of nematode

The nematode movement was observed after 24 h and 48 h, with four categories (slow, moderate, high and active) and died larvae as presented in Table 3. After 24 h in control, the highest total observed larvae were 61 with 0.0% of died larvae comparing with 25 µg/mL that detect 68 larvae with three dead larvae. In contrast, 50 µg/ml (64 observed larvae) was zero died larvae (Table 3);

meanwhile, 100 µg/mL detected 48.33% died larvae with 60 total observed larvae. On the other hand, after 48 h, results showed that the highest % of dead larva kept from 100 µg/mL concentration 53.33%, followed by 50 µg/ml 50.68%, while the lowest effect on nematode observed by 25 µg/mL (4.17%). The movement of the nematode was very high in control treatment compared with all treatments. Slow movement percentage was zero, using 25 µg/mL of Ag NPs. In comparison, using 50 and 100 µg/mL, the slow movement percentage was on average three larvae for both (5% and 4.69% respectively after 24 h), compared with the control that was zero larvae. Findings revealed that Ag NPs have the potential

**Table 3**  
Effect of Ag NPs on nematode movements after 24 and 48 h of treatments.

Treatments	Total observed larvae	Dead	Slow	%	Mod.	%	High	%	Active	%		
Ag NPs	100 µg/ml	24 h	60	29	3	5	7	11.67	21	35	0	0
	50 µg/ml		64	0	3	4.69	23	35.94	22	34.38	16	25
	25 µg/ml		68	3	0	0	8	11.76	39	57.35	18	26.47
	100 µg/ml	48 h	60	32	9	15	8	13.33	8	13.33	3	5
	50 µg/ml		73	37	0	0	3	4.10	15	20.54	18	24.66
25 µg/ml		72	3	0	0	7	9.72	60	83.33	2	2.78	
Control (Water)			61	0	0	0	0	0	0	0	61	100

to inhibit the root-knot nematode; also, these findings are in line with previous studies that NPs showed promising nematocidal activity (Kalaiselvi et al., 2019).

**4. Conclusions**

This work showed the first report of the nematocidal activity of biologically synthesized Ag NPs from *A. wilkesiana* extract against plant root-knot nematode *M. incognita*. The obtained Ag NPs have spherical shape ranging from 10 to 30 nm, and their solutions are stable at various pH values. The particle size distribution became narrower upon capping with citrate. The structural analysis with XRD, SEM, PSA, FTIR and ZP confirmed the synthesis as mentioned above method. Based on the observed data, the application of Ag NPs for combating root-knot nematodes, *Meloidogyne incognita*, could be considered promising additive, very safe materials in terms of genotoxicity, compared with the chemical nematocides products.

**Funding**

The current work was funded by Taif University Researchers Supporting Project number (TURSP-2020/85), Taif University, Taif, Saudi Arabia.

**Declaration of Competing Interest**

The authors declare that they have no known competing financial interests or personal relationships that could have appeared to influence the work reported in this paper.

**Acknowledgment**

The authors extend their appreciation to Taif University for funding current work by Taif University Researchers Supporting Project number (TURSP-2020/85), Taif University, Taif, Saudi Arabia.

**References**

Abbasi, M.W., Ahmed, N., Zaki, M.J., Shaikat, S.S., 2008. Effect of *Barleria acanthoides* Vahl. on root-knot nematode infection and growth of infected okra and brinjal plants. *Pak. J. Bot.* 40, 2193–2198.

Abd-El-Kareem, F., Elshahawy, I.E., Abd-Elgawad, M.M.M., 2021. Application of *Bacillus pumilus* isolates for management of black rot disease in strawberry. *Egypt. J. Biol. Pest Control* 31, 1–5.

Abdelkhalek, A., Al-Askar, A.A., 2020. Green synthesized ZnO nanoparticles mediated by *Mentha Spicata* extract induce plant systemic resistance against tobacco mosaic virus. *Appl. Sci.* 10 (15), 5054. <https://doi.org/10.3390/app10155054>.

Abdelkhalek, A., Al-Askar, A.A., Behiry, S.I., 2020a. *Bacillus licheniformis* strain POT1 mediated polyphenol biosynthetic pathways genes activation and systemic resistance in potato plants against Alfalfa mosaic virus. *Sci. Rep.* 10, 1–16.

Abdelkhalek, A., Salem, M.Z.M., Ali, H.M., Kordy, A.M., Salem, A.Z.M., Behiry, S.I., 2020b. Antiviral, antifungal, and insecticidal activities of Eucalyptus bark extract: HPLC analysis of polyphenolic compounds. *Microb. Pathog.* 104383.

Abdelkhalek, A., Salem, M.Z.M., Hafez, E., Behiry, S.I., Qari, S.H., 2020c. The phytochemical, antifungal, and first report of the antiviral properties of Egyptian *Haplophyllum tuberculatum* extract. *Biology (Basel)* 9 (9), 248. <https://doi.org/10.3390/biology9090248>.

Abo-Zaid, G.A., Matar, S.M., Abdelkhalek, A., 2020. Induction of plant resistance against tobacco mosaic virus using the biocontrol agent *Streptomyces cellulosa* isolate Actino 48. *Agronomy* 10 (11), 1620.

Ahamed, M., Posgai, R., Gorey, T.J., Nielsen, M., Hussain, S.M., Rowe, J.J., 2010. Silver nanoparticles induced heat shock protein 70, oxidative stress and apoptosis in *Drosophila melanogaster*. *Toxicol. Appl. Pharmacol.* 242 (3), 263–269.

Alamdari, S., Sasani Ghamsari, M., Lee, C., Han, W., Park, H.-H., Tafreshi, M.J., Afarideh, H., Ara, M.H.M., 2020. Preparation and characterization of zinc oxide nanoparticles using leaf extract of *Sambucus ebulus*. *Appl. Sci.* 10 (10), 3620. <https://doi.org/10.3390/app10103620>.

Ansari, M.J., Al-Ghamdi, A., Usmani, S., Kumar, R., Nuru, A., Singh, K., Dhaliwal, H.S., 2013. Characterization and gene mapping of a brittle culm mutant of diploid wheat (*Triticum monococcum* L.) with irregular xylem vessels development. *Acta Physiol. Plant.* 35 (8), 2407–2419.

Aziz, N., Faraz, M., Sherwani, M.A., Fatma, T., Prasad, R., 2019. Illuminating the anticancerous efficacy of a new fungal chassis for silver nanoparticle synthesis. *Front. Chem.* 7, 65.

Bhuyan, T., Mishra, K., Khanuja, M., Prasad, R., Varma, A., 2015. Biosynthesis of zinc oxide nanoparticles from *Azadirachta indica* for antibacterial and photocatalytic applications. *Mater. Sci. Semicond. Process.* 32, 55–61.

Botcha, S., Prattipati, S.D., 2019. Callus extract mediated green synthesis of silver nanoparticles, their characterization and cytotoxicity evaluation against MDA-MB-231 and PC-3 Cells. *Bionanoscience* 10 (1), 11–22.

Cromwell, W.A., Yang, J., Starr, J.L., Jo, Y.-K., 2014. Nematocidal effects of silver nanoparticles on root-knot nematode in bermudagrass. *J. Nematol.* 46, 261.

Dada, A.O., Adekola, F.A., Dada, F.E., Adelani-Akande, A.T., Bello, M.O., Okonkwo, C.R., Inyinbor, A.A., Oluyori, A.P., Olayanju, A., Ajanaku, K.O., Adetunji, C.O., 2019. Silver nanoparticle synthesis by *Acalypha wilkesiana* extract: phytochemical screening, characterization, influence of operational parameters, and preliminary antibacterial testing. *Heliyon* 5 (10), e02517. <https://doi.org/10.1016/j.heliyon.2019.e02517>.

Datta, A., Patra, C., Bharadwaj, H., Kaur, S., Dimri, N., Khajuria, R., 2017. Green synthesis of zinc oxide nanoparticles using parthenium hysterophorus leaf extract and evaluation of their antibacterial properties. *J. Biotechnol. Biomater.* 7.

El-Khatib, A.M., Badawi, M.S., Ghatass, Z.F., Mohamed, M.M., Elkhatib, M., 2018. Synthesize of silver nanoparticles by arc discharge method using two different rotational electrode shapes. *J. Clust. Sci.* 29 (6), 1169–1175.

El-Khatib, A.M., Doma, A.S., Abo-Zaid, G.A., Badawi, M.S., Mohamed, M.M., Mohamed, A.S., 2020. Antibacterial activity of some nanoparticles prepared by double arc discharge method. *Nano-Struct. Nano-Objects* 23, 100473. <https://doi.org/10.1016/j.nanos.2020.100473>.

Ghrabh, H.A., Khan, K.A., Ibrahim, E.H., Ansari, M.J., 2019. Biogenic synthesis of silver nanoparticles using Propolis Extract, their characterization, and biological activities. *Sci. Adv. Mater.* 11 (6), 876–883.

Griffiths, D., Bernt, W., Hole, P., Smith, J., Malloy, A., Carr, B., 2011. Zeta potential measurement of nanoparticles by nanoparticle tracking analysis (NTA). *NSTI-Nanotech.*, 4–7.

Gupta, M., Tomar, R.S., Kaushik, S., Mishra, R.K., Sharma, D., 2018. Effective antimicrobial activity of green ZnO nano particles of *Catharanthus roseus*. *Front. Microbiol.* 9, 2030.

Haider, M.J., Mehdi, M.S., 2014. Study of morphology and zeta potential analyzer for the silver nanoparticles. *Int. J. Sci. Eng. Res.* 5, 381–385.

Hassan, R.R.A., Mahmoud, S.M.A., Nessem, M.A., Aty, R.T.A., Ramzy, M.G., Dessoky, E. S., Abdelkhalek, A., Salem, M.Z.M., 2021. Hydroxypropyl Cellulose Loaded with ZnO Nanoparticles for Enhancing the Mechanical Properties of Papyrus (*Cyperus papyrus* L.) Strips. *BioResources* 16, 2607–2625.

Hussey, R.S., 1973. A comparison of methods of collecting inocula of *Meloidogyne* spp., including a new technique. *Plant Dis. Rep.* 57, 1025–1028.

JN, H.K.M.S., 1985. Identification of *Meloidogyne* species on the basis of differential host and perineal pattern morphology In: Barker KR Carter CC Sasser JN. *An Adv. treatise Meloidogyne* 2.

Joshi, N., Jain, N., Pathak, A., Singh, J., Prasad, R., Upadhyaya, C.P., 2018. Biosynthesis of silver nanoparticles using *Carissa carandas* berries and its potential antibacterial activities. *J. Sol-Gel Sci. Technol.* 86 (3), 682–689.

Kalaiselvi, D., Mohankumar, A., Shanmugam, G., Nivitha, S., Sundararaj, P., 2019. Green synthesis of silver nanoparticles using latex extract of *Euphorbia*

- tirucalli: a novel approach for the management of root knot nematode, *Meloidogyne incognita*. *Crop Prot.* 117, 108–114.
- Khan, M.A., Riaz, H., Raheel, M., Shakeel, Q., Waheed, U., Ahmed, N., Bashair, M., Ashraf, W., Abbas, H.T., Siddique, M., Khan, M., Naz, A., Shaheen, M., Arif, A.M., Ali, H., Nasir, M., Ansari, M.J., Ghramh, H.A., Khan, K.A., 2021. In-vitro and In-vivo management of *Meloidogyne incognita* (Kofoid and White) Chitwood and *Rhizoctonia bataticola* (Taub.) Butler in cotton using organic's. *Saudi J Biol Sci* 28 (1), 1–9.
- Khan, S.U., Anjum, S.I., Ansari, M.J., Khan, M.H.U., Kamal, S., Rahman, K., Shoaib, M., Man, S., Khan, A.J., Khan, S.U., Khan, D., 2019. Antimicrobial potentials of medicinal plant's extract and their derived silver nanoparticles: a focus on honey bee pathogen. *Saudi. J. Biol. Sci.* 26 (7), 1815–1834.
- Khan, Z., Kim, Y.H., 2007. A review on the role of predatory soil nematodes in the biological control of plant parasitic nematodes. *Appl. Soil Ecol.* 35 (2), 370–379.
- Kharisova, O.V., Dias, H.V.R., Kharisov, B.I., Pérez, B.O., Pérez, V.M.J., 2013. The greener synthesis of nanoparticles. *Trends Biotechnol.* 31 (4), 240–248.
- Kulikov, K.G., Koshlan, T.V., 2015. Measurement of sizes of colloid particles using dynamic light scattering. *Tech. Phys.* 60 (12), 1758–1764.
- Masry, S.H., Taha, T.H., Botros, W.A., Mahfouz, H., Al-Kahtani, S.N., Ansari, M.J., Hafez, E.E., 2021. Antimicrobial activity of camphor tree silver nano-particles against foulbrood diseases and finding out new strain of *Serratia marcescens* via DGGE-PCR, as a secondary infection on honeybee larvae. *Saudi J. Biol. Sci.* 28 (4), 2067–2075.
- Mohammadi-Aloucheh, R., Habibi-Yangjeh, A., Bayrami, A., Latifi-Navid, S., Asadi, A., 2018. Green synthesis of ZnO and ZnO/CuO nanocomposites in *Mentha longifolia* leaf extract: characterization and their application as anti-bacterial agents. *J. Mater. Sci. Mater. Electron.* 29 (16), 13596–13605.
- Mukherjee, S., Sau, S., Madhuri, D., Bollu, V.S., Madhusudana, K., Sreedhar, B., Banerjee, R., Patra, C.R., 2016. Green synthesis and characterization of monodispersed gold nanoparticles: toxicity study, delivery of doxorubicin and its bio-distribution in mouse model. *J. Biomed. Nanotechnol.* 12 (1), 165–181.
- Nassar, A.M.K., 2016. Effectiveness of silver nano-particles of extracts of *Urtica urens* (Urticaceae) against root-knot nematode *Meloidogyne incognita*. *Asian J. Nematol.* 5 (1), 14–19.
- Ouda, S.M., 2014. Antifungal activity of silver and copper nanoparticles on two plant pathogens, *Alternaria alternata* and *Botrytis cinerea*. *Res. J. Microbiol.* 9 (1), 34–42.
- Taha, E.H., Abo-Shady, N.M., 2016. Effect of silver nanoparticles on the mortality pathogenicity and reproductivity of entomopathogenic nematodes. *Int. J. Zool. Res.* 12 (3–4), 47–50.